Atmos. Meas. Tech., 10, 979–987, 2017
www.atmos-meas-tech.net/10/979/2017/
doi:10.5194/amt-10-979-2017

Atmospheric Measurement Techniques
Open Access
EGU

Plume propagation direction determination with SO_2 cameras

Angelika Klein, Peter Lübcke, Nicole Bobrowski, Jonas Kuhn, and Ulrich Platt

Institute of Environmental Physics, University of Heidelberg, Heidelberg, Germany

Correspondence to: Angelika Klein (angelika.klein@iup.uni-heidelberg.de)

Received: 18 August 2016 – Discussion started: 28 October 2016
Revised: 3 February 2017 – Accepted: 6 February 2017 – Published: 10 March 2017

Abstract. SO_2 cameras are becoming an established tool for measuring sulfur dioxide (SO_2) fluxes in volcanic plumes with good precision and high temporal resolution. The primary result of SO_2 camera measurements are time series of two-dimensional SO_2 column density distributions (i.e. SO_2 column density images). However, it is frequently overlooked that, in order to determine the correct SO_2 fluxes, not only the SO_2 column density, but also the distance between the camera and the volcanic plume, has to be precisely known. This is because cameras only measure angular extents of objects while flux measurements require knowledge of the spatial plume extent. The distance to the plume may vary within the image array (i.e. the field of view of the SO_2 camera) since the plume propagation direction (i.e. the wind direction) might not be parallel to the image plane of the SO_2 camera. If the wind direction and thus the camera–plume distance are not well known, this error propagates into the determined SO_2 fluxes and can cause errors exceeding 50 %. This is a source of error which is independent of the frequently quoted (approximate) compensation of apparently higher SO_2 column densities and apparently lower plume propagation velocities at non-perpendicular plume observation angles.

Here, we propose a new method to estimate the propagation direction of the volcanic plume directly from SO_2 camera image time series by analysing apparent flux gradients along the image plane. From the plume propagation direction and the known location of the SO_2 source (i.e. volcanic vent) and camera position, the camera–plume distance can be determined. Besides being able to determine the plume propagation direction and thus the wind direction in the plume region directly from SO_2 camera images, we additionally found that it is possible to detect changes of the propagation direction at a time resolution of the order of minutes. In addition to theoretical studies we applied our method to SO_2 flux measurements at Mt Etna and demonstrate that we obtain considerably more precise (up to a factor of 2 error reduction) SO_2 fluxes. We conclude that studies on SO_2 flux variability become more reliable by excluding the possible influences of propagation direction variations.

1 Introduction

Prediction and monitoring of volcanic events is highly desirable. Besides conventional methods, like seismicity or deformation measurements, continuous monitoring of volcanic gas emissions is a still relatively new method for predicting volcanic eruptions. The four most common changes in volcanic behaviour preceding an eruption are earthquakes, deformation, thermal anomalies and an increase in degassing of the volcano. Moreover, not only can an increase in degassing behaviour be an indicator of an imminent eruption, but so can a change in the composition of the volcano's degassing (see e.g. Bobrowski et al., 2015).

For short-term as well as long-term monitoring of volcanic degassing behaviour, in situ and remote-sensing techniques have been developed. While in situ techniques, such as alkaline traps and MultiGAS (Noguchi and Kamiya, 1963; Aiuppa et al., 2007) have been successfully applied, remote-sensing techniques have the particular advantage that they can be applied from a safe distance. Remote sensing started with the correlation spectrometer (COSPEC, Moffat and Millan, 1971 and Stoiber et al., 1983) but more recently the differential optical absorption spectroscopy (DOAS) technique (Platt and Stutz, 2008) is applied to volcanoes. Long-term remote-sensing monitoring of the SO_2 flux (e.g. by the Network for Observation of Volcanic and Atmospheric Change (NOVAC), Galle et al., 2010) provides insights into the standard behaviour of each individual volcano and deviations

from the normal activity can be used to predict eruptions. More recently, the SO_2 camera (e.g. Mori and Burton, 2006) that can record two dimensional SO_2 column density distributions allowed unprecedented insight into chemical and dynamic processes in volcanic plumes.

The SO_2 camera is a UV sensitive camera utilizing one or more band-pass interference filters to measure the extinction optical density (OD) of SO_2. One of those interference filters has a central transmission wavelength at about 310–315 nm. This filter is used to determine the light extinction mainly due to SO_2 and aerosols. The light extinction due to aerosol exhibits a broadband structure when compared to the narrowband structure caused by the light attenuation due to SO_2. Therefore, a second filter is applied with a central wavelength of approximately 330 nm, where the SO_2 absorption is negligible, but which is close enough to cause only small changes in light extinction by aerosol (Lübcke et al., 2013). From the logarithm of the (suitably normalized) pixel-per-pixel ratio of two images taken through either filter, images of the SO_2 OD can be calculated. The SO_2 OD in turn is proportional to the SO_2 column density along the line of sight.

The propagation velocity of the plume and the distance between the plume and the camera are two important variables used to determine the SO_2 flux from volcanoes using imaging data. Usually the apparent propagation velocity (i.e. the angular velocity) of the plume can be derived directly from the camera image series. For that purpose, one correlates two integrated transects of the trace gas slant column density images of the moving plume and determines the time lag between the two signals (McGonigle et al., 2005). One can determine the velocity of the plume from the time lag, the angular distance between the two image columns and the distance of the plume. While this method is simple to implement, it only provides a spatial and temporal mean propagation velocity that neglects, for example, turbulence or propagation velocity variations over the extent of the plume. A more detailed plume velocity determination can be achieved using optical flow algorithms (Kern et al., 2015b). These algorithms determine the displacement of image intensity values for each pixel from one frame to the next frame, thus giving a detailed spatial and temporal plume velocity estimation if the direction of the plume is known.

In any case, an important prerequisite for the determination of absolute trace gas flux values is the precise knowledge of the distance between the plume and observing instrument (usually the SO_2 camera).

This distance is usually more difficult to (precisely) determine than it is generally assumed: while the geographic locations of the volcanic gas source (i.e. usually the crater) and the position of the instrument are almost always precisely known, the plume propagation direction (like the plume velocity) is not. It is advantageous to know the propagation direction of the plume to achieve a good estimation of the plume distance. This usually requires additional measurements, which are often hard to make at volcanoes due to the limited infrastructure. This paper is about the possibility of determining the plume propagation direction itself from a time series of SO_2 camera images of a volcanic plume.

2 Theory

The trace gas flux Φ is approximated from 2-D imaging data following the equation

$$\Phi = \boldsymbol{v} \cdot \sum_i h_i \cdot S_i. \quad (1)$$

here, $\boldsymbol{v}$ is the propagation velocity of the plume perpendicular to the viewing direction, h_i is a side length of a pixel at the distance of the plume and S_i denotes the SO_2 column densities of each respective pixel. The summation of the length of every pixel in the plume transect gives the overall diameter of the plume. The summation over every column density of these pixels gives the column density of the complete transect.

If the volcanic SO_2 plume moves within the image plane, the camera captures a scaled image of the field of view (FOV) of the camera image, with a scaling factor that is dependent on the plume distance. Thus, the diameter of the plume and its propagation velocity can be easily calculated once the plume distance is known. In a simplified approach which neglects radiation transport issues (as described e.g. by Kern et al., 2010) the column densities S_i depend linearly on the length of the light path through the plume. For a cylindrically symmetric plume moving parallel to the object plane, the detector pixels at the centre of the plume capture column densities corresponding to the SO_2 concentration integrated along the plume diameter, while the detector pixels towards the border of the plume capture the light path along secants of the plume (see Fig. 1). Since the secants are not exactly parallel to the radius this causes an overestimation of the measured SO_2 column densities towards the edges of the detector. Furthermore, if the plume is inclined (by the angle α, see Fig. 1) with respect to the image plane, deviations in the SO_2 flux determination of the plume will occur even in the centre of the image plane. In the following sections different approaches to take the geometry into account during the calculation of SO_2 fluxes will be discussed. The angle between the image plane and the tilted plume will be referred to as inclination angle α. The inclination of the plume changes all the measured variables in Eq. (1).

2.1 Small FOV angle approach

In a first simplified approach for a small FOV angle of a few degrees, the inclination deviations are negligible (below 10 % change in SO_2 flux at α smaller than 2°). Figure 1 shows a schematic sketch of the geometry of the set-up of an inclined plume. The actual plume extent in x direction x_R of a tilted plume imaged with the SO_2 camera is longer than the apparent plume extent x_M projected on the image plane. It can be

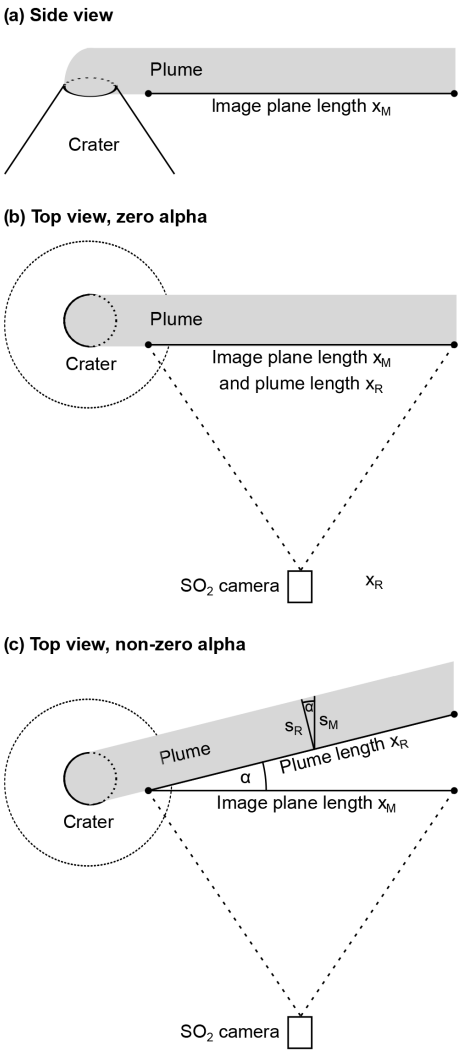

Figure 1. Schematic view on the influence of the inclination of the plume on the measured variables for the SO_2 flux determination for an SO_2 camera with a small FOV angle. **(a)** Side view of the volcanic plume and **(b)** top view of a volcanic plume parallel to the image plane, **(c)** top view of a plume inclined with respect to the image plane.

calculated as

$$x_R = \frac{x_M}{\cos\alpha}. \tag{2}$$

The true plume velocity v_R (in x direction) depends linearly on the plume extent ($v_R = \frac{x_R}{t} = \frac{x_M}{\cos(\alpha)t} = \frac{v_M}{\cos(\alpha)}$).

In contrast to the apparent underestimation of the plume velocity, the measured column densities S_M for an inclined SO_2 plume are larger than the perpendicular column densities S_R. The column density correction follows the equation

$$S_R = S_M \cdot \cos\alpha. \tag{3}$$

The column densities depend linearly on the light path s through the plume in a first order approximation for a homogeneous plume with an SO_2 concentration c ($S = c \cdot s$). Therefore, Eq. (3) can be rewritten as

$$s_R = s_M \cdot \cos\alpha. \tag{4}$$

In this first assumption (FOV $\leq 2°$) the deviations in the velocity and in the column density would cancel each other out in the flux calculation (see Eq. 1) as already noted by Mori and Burton (2006). Only the apparent plume diameter h_M (i.e. the vertical extent of the plume in the direction of the y axis) would be affected and thus deviate from the true plume diameter h_R, since the actual distance of the plume differs from the assumed distance, which causes a wrong scaling of the plume diameter on the image plane.

$$h_R = h_M + \frac{1}{2} \cdot x_M \cdot \tan\alpha \tag{5}$$

It should be noted that the x_R and s_R over- and underestimations nearly cancel each other out for SO_2 cameras with a small FOV angle but also for a chosen small FOV angle within the large FOV angle of an SO_2 camera. However, the distance of the plume still needs to be known to determine the correct plume diameter and thus also the information about the propagation direction of the plume is a necessary prerequisite even in this approach.

2.1.1 Large FOV angle approach

Usually, SO_2 cameras have a relatively large FOV angle γ (typically several 10°, Fig. 2). Therefore, a more realistic approach includes the angular aperture of the FOV in the determination of the variation of the variables in Eq. (1).

For FOV angles of the SO_2 camera larger than 2°, the apparent plume extent in x direction and column densities are affected in a way that is different from the previous approach, when the plume is tilted with respect to the image plane (i.e. at non-zero alpha).

The plume length deviation equation (Eq. 2) changes if the FOV projection is taken into account. Additionally to the deviations x_K of an orthographic projection (every distance is projected with the same magnification factor, see grey section in plume length x_R in Fig. 2), the perspective projection leads to an addition of a length x'_K (see red section in plume length x_R in Fig. 2) for a plume moving away from the observer ($\alpha > 0$) and subtraction of x'_K (i.e. x'_K becoming negative) if the plume moves towards the observer ($\alpha < 0$). The additional length x'_K can be calculated with the law of sines.

$$x_K = \frac{x_M}{\cos\alpha} \tag{6}$$

$$\frac{x'_K}{\sin\gamma} = \frac{q}{\sin(90° - \alpha - \gamma)} = \frac{x_M \cdot \tan\alpha}{\sin(90° - \alpha - \gamma)} \tag{7}$$

$$\rightarrow x'_K = \frac{x_M \cdot \sin\gamma \tan\alpha}{\sin(90° - \alpha - \gamma)} \tag{8}$$

$$x_R = \frac{x_M}{\cos\alpha} \cdot \left(1 + \frac{\sin\gamma \sin\alpha}{\sin(90° - \alpha - \gamma)}\right) \tag{9}$$

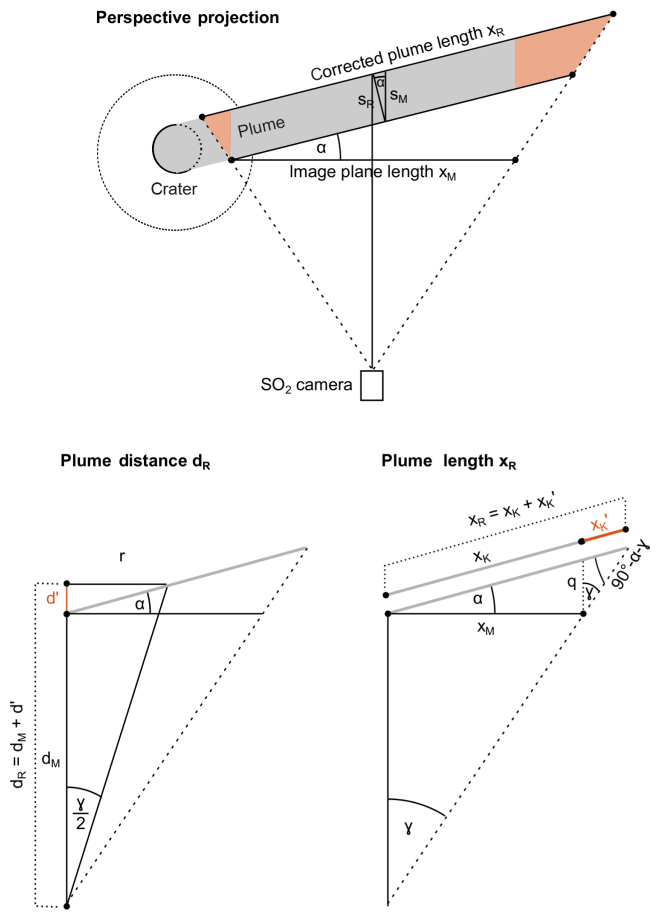

Figure 2. Schematic sketch of the influence of a large FOV angle on the deviation of the plume length x_R from the assumed plume length x_M and on the plume distance d_R from the assumed plume distance d_M. The additional distance the plume travels in comparison to the case of a plume moving away from the camera ($\alpha = 0$) is marked in red. Here, only the case of a plume moving away from the camera ($\alpha > 0$) is shown.

Equation (9) can be rewritten as Eq. (10). Besides the scaling with $\cos\alpha$ from the small FOV angle approach (see Eq. 2), an additional term describes the influence of the FOV angle γ on x_R.

$$x_R = \frac{x_M}{\cos\alpha}\left(1 - \frac{\tan(\gamma)\tan(\alpha)}{1+\tan(\gamma)\tan(\alpha)}\right) \tag{10}$$

Additionally, the length of the slant beam through the plume is not only dependent on the tilt angle α but also on the FOV angle γ of the respective pixel following equation

$$s_R = s_M \cdot \cos\left(\alpha + \frac{\gamma}{2}\right). \tag{11}$$

The distance of the plume also changes for every FOV angle in dependence of the inclination of the plume.

$$d_R = \frac{r}{\tan\left(\frac{\gamma}{2}\right)} = \tan\alpha \cdot r + d_M \tag{12}$$

$$r = \tan\left(\frac{\gamma}{2}\right)\tan\alpha \cdot r + \tan\left(\frac{\gamma}{2}\right)\cdot d_M \tag{13}$$

$$r \cdot \left(1 - \tan\left(\frac{\gamma}{2}\right)\tan\alpha\right) = \tan\left(\frac{\gamma}{2}\right)\cdot d_M \tag{14}$$

$$r = \frac{\tan\left(\frac{\gamma}{2}\right)\cdot d_M}{1 - \tan\left(\frac{\gamma}{2}\right)\tan\alpha} \tag{15}$$

$$d_R = \frac{\tan\left(\frac{\gamma}{2}\right)\cdot d_M}{\tan\left(\frac{\gamma}{2}\right)\cdot\left(1 - \tan\left(\frac{\gamma}{2}\right)\tan\alpha\right)} \tag{16}$$

$$d_R = \frac{d_M}{1 - \tan\left(\frac{\gamma}{2}\right)\tan\alpha} \tag{17}$$

Figure 3 shows the deviations of the tilt-corrected values of the variables (with index R) from the measured values of the variables (indicated by the index M) as a function of the inclination angle α. The distance of the plume in the midst of the FOV is known but since the direction of the plume is not known, the distances in other positions of the image are also not known. The camera's FOV angle is chosen as 24° which is in the range of commonly used SO_2 camera FOV today (Kern et al., 2015a). The graphs show the deviations for half of the image plane from its centre to an angle $\gamma/2$ of 12° where half of the image plane is assumed to be a single detector pixel. An orthographic projection (produced by a telecentric optical set-up; e.g. Jähne, 2005) leads to the blue lines in Fig. 3. Its characteristic is that an object is projected to be the same size independent of its distance to the camera. The red lines in Fig. 3 represent the deviations due to a perspective projection that is used in SO_2 camera measurement set-ups. The projected size of an object is dependent on the distance for a perspective projection. Figure 4 shows the combined deviations that would influence the flux determination.

These calculations cover half of the actual FOV angle of the camera. If the plume is inclined with the angle α towards the image plane, it is tilted by a negative angle $-\alpha$ for the respective other half of the FOV. Therefore the over- and underestimations of the actual SO_2 flux differ on both sides of the field of view.

Usually the SO_2 camera detectors consist of several hundred pixels. Equation (18) represents the deviations in the plume length and therefore in the plume propagation velocity if the FOV angle is divided in a finite absolute number of pixels p for every pixel i in p.

$$x_R(i, x_M) = \frac{x_M}{\cos\alpha}\left[1 + i^2\frac{\tan\gamma\tan\alpha}{p - i\tan\gamma\tan\alpha} - (i-1)^2\frac{\tan\gamma\tan\alpha}{p-(i-1)\tan\gamma\tan\alpha}\right] \tag{18}$$

Equation (19) represents the deviations in the measured column densities if the FOV angle is divided in a finite absolute number of pixels p for every pixel i in p.

$$s_R(i, s_M) = s_M \cdot \cos\left[\alpha + \tan^{-1}\left(\frac{i-1}{p}\tan\gamma\right)\right.$$

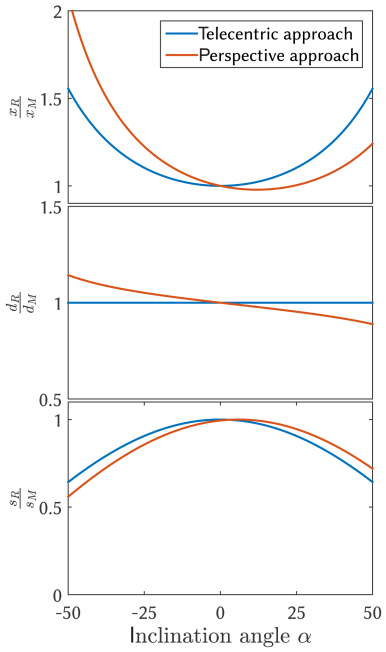

Figure 3. Mean deviations of the plume extent in the x direction (x_R), plume distance (d_R) and column density (s_R), used in the flux determination for the right half of the image plane of an SO_2 camera with an FOV angle of 24° (for the left half of the detector the inclination deviations would be vice versa). The blue lines show the ratio between the ground truth (i.e. the geometric accurate) variables and the measured variables for a telecentric (an orthographic projection where the apparent size does not depend on the distance) approach. The red lines show the same ratio for a perspective approach.

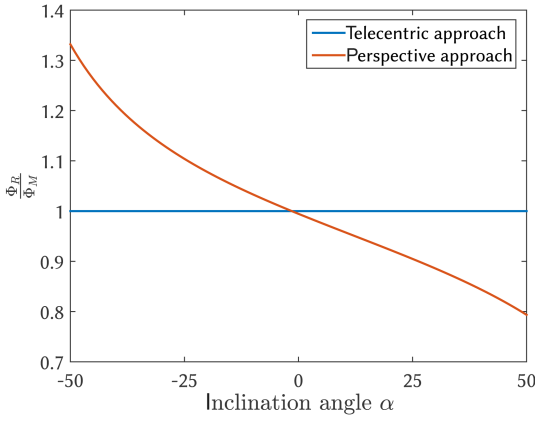

Figure 4. Combined deviations of the three variables of the flux determination for the right half of the image of an SO_2 camera with an FOV angle of 24°.

$$-\frac{1}{2}\cdot\tan^{-1}\left(\frac{i}{p}\tan\gamma\right)\Bigg] \tag{19}$$

Equation (20) represents the deviations in the measured distance for every pixel i for a tilted plume.

$$d_R(i,d_M) = \frac{d_M}{1-\tan\alpha\tan\left[\tan^{-1}\left(\frac{i-1}{p}\tan\gamma\right)-\frac{1}{2}\cdot\tan^{-1}\left(\frac{i}{p}\tan\gamma\right)\right]} \tag{20}$$

If we want to determine the plume propagation direction, we can measure the SO_2 flux for a given distance at different positions of the plume. If the apparent SO_2 flux is the same at different positions in the plume, the plume lies within the image plane. Otherwise we observe an apparent gradient in the measured flux across the image, which, however, contains information on the plume propagation direction. Dividing the measured fluxes by the respective deviations for the investigated pixel columns for every possible tilt angle α and minimizing the observed gradient yields the information about the mean plume propagation direction during the time period needed for the parcel to move across the field of view. The assumption that the SO_2 flux is conserved can be made since the mean lifetime of SO_2 in the troposphere is usually of the order of several days (e.g. Eisinger and Burrows, 1998) while the typical time for the plume to cross the field of view of the camera is of the order of a few minutes. Note that the SO_2 flux originating from the volcano should vary for our method to work. The second necessary prerequisite is that the advective transport is larger than the turbulent transport of the plume parcel. Kern (2009) showed that usually the turbulent transport only contributes to about 0.2 % of the gas transport in the plume.

Figure 5 shows the deviation in each measurement variable separately for an SO_2 camera, again with a typical FOV of 24°, while Fig. 6 shows the combined deviation of the flux measurement due to the perspective influence on the three variables. For an SO_2 camera with a typical FOV of 24° the deviations in the ratio $\frac{x_R}{x_M}$ easily exceed 50 % at plume direction tilts of $> 30°$. As a consequence, the SO_2 flux deviation already exceeds 10 % in parts of the SO_2 camera images for a plume tilt angle larger than 15°.

Equations (18), (19) and (20) are defined for the case that the best known distance between the observer and the plume is in the centre of the FOV. If the best known distance is not in the centre of the FOV, the equations can be adjusted since the distance correction d_R and the inclination velocity correction x_R change (see also Fig. 7).

With n as the number of pixels, the known position is shifted to the side of the FOV, we can derive the new distance of the centre of the FOV as

$$d'_M = d_M + d_P \tag{21}$$

$$d_P = n\cdot x_M\cdot\tan\alpha = \frac{n}{p}\cdot d_M\cdot\tan\gamma\tan\alpha \tag{22}$$

$$d'_M = d_M\cdot\left(1+\frac{n}{p}\tan\alpha\tan\gamma\right). \tag{23}$$

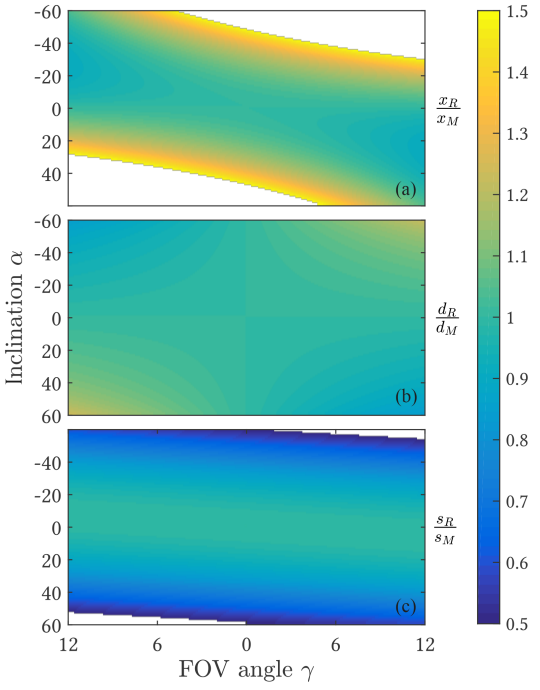

Figure 5. Ratio of the real variables to the measured variables of the velocity (upper panel), plume distance or diameter (middle panel) and column densities (lower panel) for an SO_2 camera with an FOV angle of 24°. The relative deviations of distance are the same as for the diameter ($\frac{h_R}{h_M} = \frac{d_R}{d_M}$). Relative deviations larger than 0.5 from the measured data are shaded white.

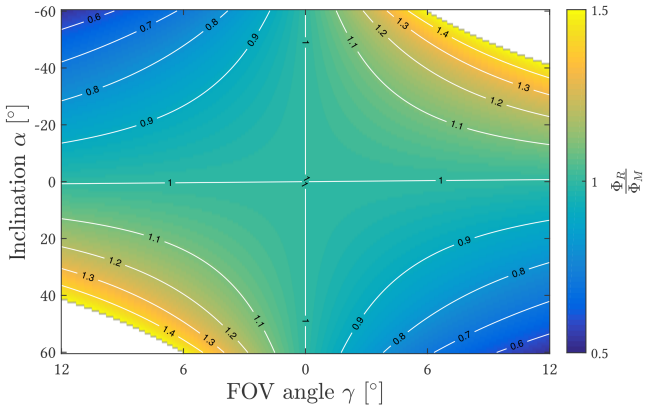

Figure 6. Deviation of the total true flux from the measured flux (with no inclination assumed) as a function of the FOV angle of the SO_2 camera and the inclination angle α. A perspective imaging of a plume with unknown inclination can lead to wrong flux estimations. Deviations larger than 0.5 from the measured data are shaded white. White stripes show the 0.1 steps of the deviations.

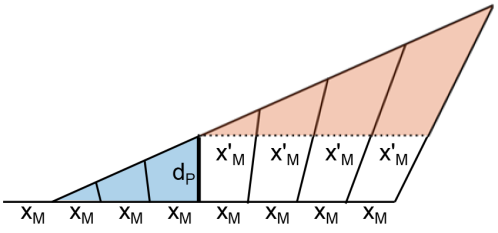

Figure 7. Schematic drawing of the shift of the best known distance towards the border of the image array. The equations for the perspective correction can be adapted to the respective position of the best known distance.

Accordingly the new measured lengths of the pixels x'_M can be calculated as

$$x'_M = x_M \cdot \left(1 + \frac{n}{p} \tan\alpha \tan\gamma\right). \quad (24)$$

3 Application

We used the considerations developed in Sect. 2 (together with the usually well-justified assumption of a constant SO_2 flux) to design an algorithm which allows us to determine the wind direction directly from SO_2 camera plume images without the need for further data or assumptions. The new algorithm has been applied to an SO_2 camera measurement data set taken at Mt Etna, Sicily on 9 July 2014. Not only the possibility of the inclination angle estimation, but also the possibility of observation of a wind direction change, was investigated. Figure 8 shows the geometry of the data set.

3.1 Plume propagation direction determination

Figure 9 shows the SO_2 fluxes at three different positions in the FOV of the SO_2 camera for a measurement data set taken at Mt Etna. The upper panel shows the SO_2 flux for each of these positions not corrected for inclination. The lower panel shows the fluxes corrected for the inclination. During the measurement campaign, in addition to the SO_2 camera measurements, measurements were taken by a car-based DOAS instrument pointing to the zenith and traversing the plume (see e.g. McGonigle et al., 2002; Galle et al., 2003). The centre of the plume can be found by evaluating the SO_2 column density and determining the location with the maximum values. Thus, the wind direction could be estimated, giving an inclination of the plume of about 38°. This information was then used to verify the applicability of the developed algorithm to the SO_2 camera data sets. Figure 10 shows the fluxes at seven different positions in the camera image from the data set taken at Etna on 9 July 2014. The SO_2 flux was calculated assuming different plume inclination angles. Figure 10 shows that the SO_2 fluxes are nearly the same if the plume is tilted about 40° in the backward direction with an uncertainty of ±5°. This result agrees with the result from the traverse measurements within a margin of ±2°.

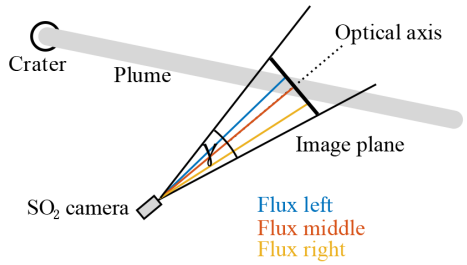

Figure 8. Map of the geometrical set-up of the measurement data set. The inclination of the plume is 38° with respect to the image plane. The positions in the FOV used for the flux determination are coloured.

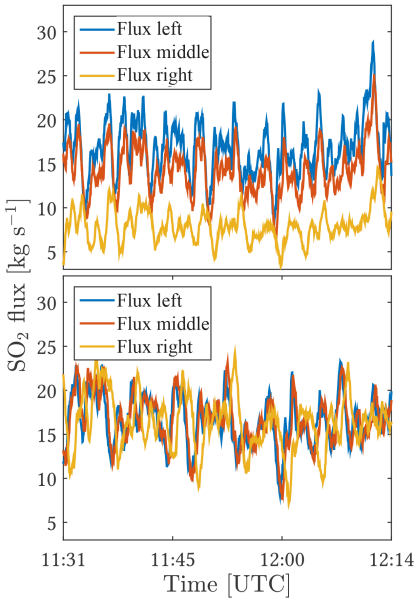

Figure 9. Deviations of the SO_2 fluxes of three different cross sections through the plume. These apparent deviations are caused by the unknown inclination of the plume with respect to the image plane. This measurement set was taken at Mt Etna on the 9 July 2014.

3.2 Real-time tracking of changes in the wind direction

If there are changes in the propagation direction of the plume during SO_2 camera measurements, it is possible to detect these changes on timescale of minutes. Figure 11 shows a change in the ratio between the apparent SO_2 flux determined in two different positions of the plume within the FOV of the camera. During 2 h of measurements between 11:32 and 13:23 UTC, on 9 July 2014, the wind direction was stable for about 1 h (A). For this period the ratio between the two flux measurement positions was mostly constant, except for slight fluctuations. Then the inclination angle changed by about 20°, which we attribute to a change of the wind direction (B). In this phase of the observation the ratio between the two flux measurements is decreasing. Later, the new wind

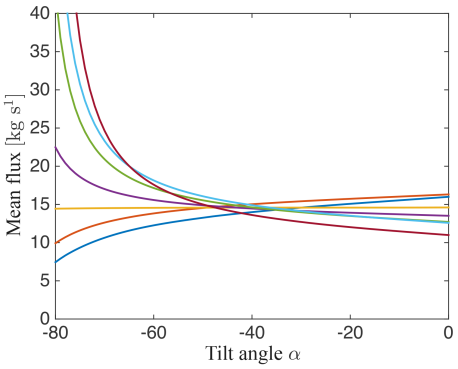

Figure 10. Mean fluxes of seven different cross sections of the measurement data set as a function of the angle correction. Each cross section is plotted in a different colour. The SO_2 flux should be the same in each cross section if it is a conservative tracer. The plume inclination can be estimated to 40° with an uncertainty of 5°. Along with knowing the orientation of the camera set-up, this information can be used to determine the plume propagation direction.

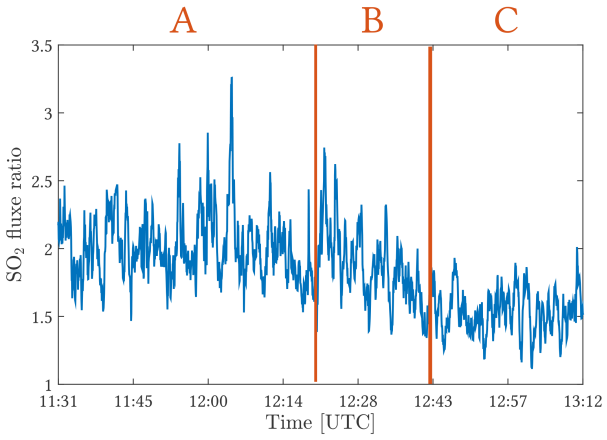

Figure 11. Observation of a wind direction change using the apparent flux ratios of two different cross sections of the plume which were corrected for the perspective. Depending on the propagation velocity, it is possible to determine direction changes on a timescale of minutes. For every inclination towards the image plane, the ratio of the fluxes is unique. On this data set, there occurred a direction change after phase A at 12:26 UTC. The wind direction in phase A was $281 \pm 5°$. The direction change of about 20° in phase B took approximately 23 min. A new stable propagation direction of $301 \pm 5°$ established in phase C at 12:49 UTC.

direction stabilizes in (C), with a new constant ratio between the two flux measurements. The SO_2 plume also exhibits a slight contribution due to turbulent transport. The turbulent transport usually contributes less than 0.2 % to the propagation of the plume (Kern, 2009).

4 Conclusions

We showed that an inclined plume causes apparent spatial flux gradients in the SO_2 camera measurement images. The frequently implicitly (e.g. Smekens et al., 2015) or explicitly (e.g. Mori and Burton, 2006) assumed compensation effect only occurs at very small inclination angles ($< 15°$) or small FOV ($< 2°$). For an SO_2 camera with an FOV angle of 24° a tilt angle of 15° already causes flux deviations larger than 10 % in parts of the SO_2 camera's images for evaluations relying on the compensation effect. However, these gradients are unambiguous for every possible inclination angle of the volcanic plume with respect to the image plane of the SO_2 camera. Therefore, they can not only be corrected but can also be used to determine the direction of the plume (i.e. the wind direction at the location of the plume). On longer timescales that exceed the travel time of the plume parcel across the FOV (several minutes), even the change in the mean wind direction can be observed. On the other hand, if these errors in plume inclination are ignored they can give rise to erroneous observations of fluxes, in particular fake flux changes with plume age or over time can occur. If these changes in flux are attributed to chemical processes in plumes (e.g. SO_2 oxidation) or of volcanic degassing patterns, the wrong conclusions with respect to chemical processes in volcanic plumes or wrong interpretation on degassing behaviour may be drawn.

While the proposed algorithm is applicable to straight and bent plumes (i.e. plumes where the wind direction changes within the field of view), so far the combined effects of this study and radiative transfer issues have not yet been addressed. Additionally, if several plumes are masking each other, the proposed algorithm may not work.

Recent improvements in the velocity determination of volcanic plumes using image processing methods like optical flow algorithms can be combined with the proposed perspective correction method for a robust SO_2 flux determination.

5 Data availability

The raw measurement data (spectra and images, more than 1 GB in size) of the SO_2 camera can be obtained on request from the authors.

Competing interests. The authors declare that they have no conflict of interest.

Acknowledgements. We acknowledge the work of Sebastian Illing and Marco Huwe on the SO_2 camera prototype that was used for the Mt Etna measurements.

Further, the authors thank for the financial support from the DFG project "DFG BO 3611/1-2".

We acknowledge the financial support of the Deutsche Forschungsgemeinschaft and Ruprecht-Karls-Universität Heidelberg within the funding programme Open Access Publishing.

Edited by: T. von Clarmann
Reviewed by: three anonymous referees

References

Aiuppa, A., Moretti, R., Federico, C., Giudice, G., Gurrieri, S., Liuzzo, M., Papale, P., Shinohara, H., and Valenza, M.: Forecasting Etna eruptions by real-time observation of volcanic gas composition, Geology, 35, 1115–1118, doi:10.1130/G24149A.1, 2007.

Bobrowski, N., von Glasow, R., Giuffrida, G. B., Tedesco, D., Aiuppa, A., Yalire, M., Arellano, S., Johansson, M., and Galle, B.: Gas emission strength and evolution of the molar ratio of BrO/SO_2 in the plume of Nyiragongo in comparison to Etna, J. Geophys. Res.-Atmos., 120, 277–291, doi:10.1002/2013JD021069, 2015.

Eisinger, M. and Burrows, J. P.: Tropospheric sulfur dioxide observed by the ERS-2 GOME instrument, Geophys. Res. Lett., 25, 4177–4180, doi:10.1029/1998GL900128, 1998.

Galle, B., Oppenheimer, C., Geyer, A., McGonigle, A. J., Edmonds, M., and Horrocks, L.: A miniaturised ultraviolet spectrometer for remote sensing of SO_2 fluxes: a new tool for volcano surveillance, J. Volcanol. Geoth. Res., 119, 241–254, doi:10.1016/S0377-0273(02)00356-6, 2003.

Galle, B., Johansson, M., Rivera, C., Zhang, Y., Kihlman, M., Kern, C., Lehmann, T., Platt, U., Arellano, S., and Hidalgo, S.: Network for Observation of Volcanic and Atmospheric Change (NOVAC) – A global network for volcanic gas monitoring: Network layout and instrument description, J. Geophys. Res.-Atmos., 115, D05304, doi:10.1029/2009JD011823, 2010.

Jähne, B.: Digital Image Processing, 6th edition, Springer Berlin Heidelberg, Germany, 2005.

Kern, C.: Spectroscopic measurements of volcanic gas emissions in the ultra-violet wavelength region, Dissertation, Institute of Environmental Physics, The Faculty of Physics and Astronomy, University Heidelberg, doi:10.11588/heidok.00009574, 2009.

Kern, C., Kick, F., Lübcke, P., Vogel, L., Wöhrbach, M., and Platt, U.: Theoretical description of functionality, applications, and limitations of SO_2 cameras for the remote sensing of volcanic plumes, Atmos. Meas. Tech., 3, 733–749, doi:10.5194/amt-3-733-2010, 2010.

Kern, C., Lübcke, P., Bobrowski, N., Campion, R., Mori, T., Smekens, J.-F., Stebel, K., Tamburello, G., Burton, M., Platt, U., and Prata, F.: Intercomparison of SO_2 camera systems for imaging volcanic gas plumes, J. Volcanol. Geoth. Res., 300, 22–36, doi:10.1016/j.jvolgeores.2014.08.026, 2015a.

Kern, C., Sutton, J., Elias, T., Lee, L., Kamibayashi, K., Antolik, L., and Werner, C.: An automated SO_2 camera system for continuous, real-time monitoring of gas emissions from Klauea Volcano's summit Overlook Crater, J. Volcanol. Geoth. Res., 300, 81–94, doi:10.1016/j.jvolgeores.2014.12.004, 2015b.

Lübcke, P., Bobrowski, N., Illing, S., Kern, C., Alvarez Nieves, J. M., Vogel, L., Zielcke, J., Delgado Granados, H., and Platt, U.: On the absolute calibration of SO_2 cameras, Atmos. Meas. Tech., 6, 677–696, doi:10.5194/amt-6-677-2013, 2013.

McGonigle, A. J. S., Oppenheimer, C., Galle, B., Mather, T. A., and Pyle, D. M.: Walking traverse and scanning DOAS measurements of volcanic gas emission rates, Geophys. Res. Lett., 29, 46–1–46–4, doi:10.1029/2002GL015827, 2002.

McGonigle, A. J. S., Hilton, D. R., Fischer, T. P., and Oppenheimer, C.: Plume velocity determination for volcanic SO_2 flux measurements, Geophys. Res. Lett., 32, L11302, doi:10.1029/2005GL022470, 2005.

Moffat, A. J. and Millan, M. M.: The applications of optical correlation techniques to the remote sensing of SO_2 plumes using sky light, Atmos. Environ., 5, 677–690, doi:10.1016/0004-6981(71)90125-9, 1971.

Mori, T. and Burton, M.: The SO_2 camera: A simple, fast and cheap method for ground-based imaging of SO_2 in volcanic plumes, Geophys. Res. Lett., 33, L24804, doi:10.1029/2006GL027916, 2006.

Noguchi, K. and Kamiya, H.: Prediction of volcanic eruption by measuring the chemical composition and amounts of gases, Bull. Volcanol., 26, 367–378, doi:10.1007/BF02597298, 1963.

Platt, U. and Stutz, J.: Differential Absorption Spectroscopy, in: Differential Optical Absorption Spectroscopy: Principles and Applications, 135–174, Springer Berlin Heidelberg, Berlin, Heidelberg, doi:10.1007/978-3-540-75776-4_6, 2008.

Smekens, J.-F., Burton, M. R., and Clarke, A. B.: Validation of the SO_2 camera for high temporal and spatial resolution monitoring of SO_2 emissions, J. Volcanol. Geoth. Res., 300, 37–47, doi:10.1016/j.jvolgeores.2014.10.014, 2015.

Stoiber, R., Malinconico, L., and Williams, S.: Use of the correlation spectrometer at volcanoes, Forecasting volcanic events, 1, 425–444, 1983.